Wideband high-*Q* nonlinear resonance for MEMS

J. V. Clark, Y. Han, A. Abrol, Z. Zun

Electrical and Computer Engineering
Mechanical Engineering
Auburn University, USA

ABSTRACT

We examine high quality factor (*Q*) nonlinear wide-bandwidth resonance for microelectromechanical systems (MEMS) by mimicking high nonlinearity in stiffness by force feedback. The *Q* and bandwidth are usually thought of as being inversely proportional to each other for linear systems, where a large *Q* is achieved with a narrow bandwidth, and vice versa. However, by invoking a feedback force that mimics highly nonlinear stiffness, we demonstrate that it may be possible to achieve the behavioral benefits of both large amplitude and wide bandwidth. As a test case, we demonstrate how this concept may benefit devices that suffer from thermal drift or mode mismatch, such as MEMS vibratory gyros.

Keywords: nonlinear stiffness, high-*Q*, wideband, wide bandwidth, force feedback, PODMEMS

1. INTRODUCTION

MEMS (microelectromechanical systems) resonators with high sensitivities can be susceptible to noise. To achieve a stronger signal to noise ratio (SNR), larger displacement amplitudes are usually required. Increasing the quality factor (*Q*) is a most common way to achieve a large deflection. During the MEMS design process, *Q* is often increased by either optimizing the structural design to minimize thermoelastic energy dissipation, increasing the proof mass, or by reducing ambient damping. The benefit of higher *Q* is illustrated in **Figure 1**, where it is shown that a higher *Q* results in a lower bias [1]. For comparison, the rotation rate of the earth is 15°/hr.

For linear systems, the *Q* of a *vertical pole* is estimated as $Q = \omega_p / BW$, where ω_p is the pole frequency and *BW* is the bandwidth of the vertical pole. For such systems, achieving a large *Q* requires a very small *BW* or a very large ω_p. Issues from a small BW include thermal drift and mismatch. Thermal drift (from fluctuations in temperature) shifts the resonant frequency of the structure away from the driving frequency of the electronics. Mismatch (between the resonant frequencies of the drive and sense modes of vibratory gyros) stems from process variation, packaging stresses, thermal drift, and aging. For high *Q*s having small

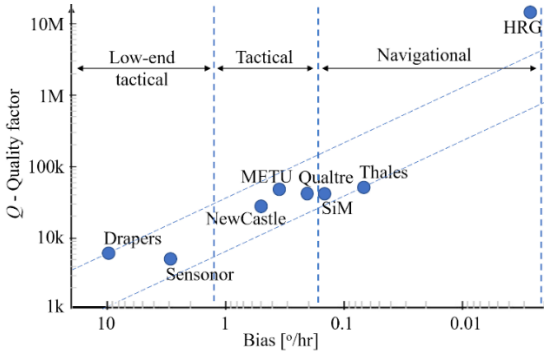

Figure 1: Quality factor vs. bias for a variety of MEMS gyros. The trend shows that a higher *Q* can result in a smaller bias. The data in the plot is from [1].

BWs, mismatch between the electrical drive frequency and the drifting mechanical frequency, or mismatch between the resonant frequencies of the drive mode and sense mode, can significantly attenuate the SNR, resulting in poor performance. For instance, a mismatch of 1Hz for a gyro having a ω_p of 15kHz and *Q* of 75k can worsen its angle random walk (ARW) by an order of magnitude [7].

There have been several efforts by researchers to reduce the effects of drift and mismatch in gyros for improved SNR leading to a reduced ARW. These efforts include increasing the size of the bandwidth while trading off *Q*; automatic gain control (AGC) to maintain a significant amplitude during small frequency shifts [2]; phase-locked loop (PLL) to track a drifting resonant frequency [3]; AGC and PLL combined to the drive and sense modes of a gyro [5]; Lyapunov-based adaptive control to specify the value of resonant frequency in [4]; automatic mode matching through disturbance rejection based closed-loop control [6]; mode matching by adding nanoparticle ink droplets to the proof mass [7]; and automatic mode matching by applying a negative electrostatic stiffness tuning to the sense mode to within 0.1Hz [8].

In this paper, we consider the possibility of mode matching and insensitivity to thermal drift for vibratory gyros by enacting an early onset of high nonlinearity in stiffness to achieve simultaneous high-*Q* and high-BW. This is done by using electrostatic feedback to mimic the Duffing oscillator [9] for the drive and sense modes. By doing so, a pole that would be vertical in a linear system will be curved to the right (for stiffness hardening) or left (for stiffness

softening) in this nonlinear system. In addition, we suggest that such a curved pole can be exploited as a type of effective bandwidth. Since we define bandwidth differently here, we use the general definition of *Q*, which is the ratio of the maximum energy stored to the energy dissipated per cycle.

Our method and model for nonlinear stiffness control using electrostatic force feedback is presented in Section 2. The effect of thermal drift upon linear and nonlinear versions of our model is explored in Section 3. And the effect of mismatch upon linear and nonlinear version of our model is explored in Section 4. This preliminary analysis suggests that nonlinear stiffness control by electrostatic force feedback is able to achieve both high *Q* and wide bandwidth, which might be useful for addressing the problem of drift or mismatch in vibratory gyros.

2. NONLINEAR STIFFNESS MODEL

In this section we present our method and model for nonlinear stiffness control using electrostatic force feedback. Our method for the linear type of performance control was presented in [11]. The method, called POD (performance on demand) or PODMEMS, involves monitoring the instantaneous state of the proof mass in real time, and immediately feeding back an electrostatic force onto the proof mass that is proportional to its displacement, velocity, or acceleration. In doing so, the overall effective mass, damping, or stiffness of the system appears to be controllably increased or decreased.

This paper extends our prior study of PODMEMS to the nonlinear regime by feeding back an electrostatic force onto the proof mass that is proportional to cubic displacement to produce the nonlinear characteristics of the Duffing equation. The governing equation of motion of the system can be described as

$$M\ddot{x} + D\dot{x} + Kx + \kappa_e x_\tau^3 = F_{dr} + F_{ext} \quad (1)$$

where *M* is the proof mass, *D* is damping, *K* is stiffness, F_{dr} is the driving force, F_{ext} is the external force, and κ is the coefficient of nonlinear stiffness. Unlike $\kappa\, x^3$, the term $\kappa_e x_\tau^3$ is not due to mechanics, it is due to the electrostatic feedback force $F_{fb}(x,\tau)$ which is a function of the displacement of the proof mass and the delay (or reaction time) of the feedback circuit. The displacement x_τ is the location of where the proof mass used to be τ seconds ago. That is, $x_\tau = x(t-\tau)$. Analog feedback circuits produce a slight delay τ, which is on the order of $O(10^{-8})$ seconds, which is acceptable for MEMS operating below ~MHz. If the delay is too large, instability can result [11]. The delay is from the totality of RC time constants and parasitic inductances in the processing circuit that cause the displacement that was sensed at time t to be converted to into a feedback force that is applied at time $t+\tau$.

For transient analysis, because equation (1) is in part a function of a prior state, it is a delay differential equation (DDE), which requires a specialized DDE solver. Most ordinary differential equation solvers are not able to accurately solve DDEs. In the following analysis, we examine the steady-state condition and assume that τ is small enough so that the system is stable [11].

For a test case, we consider the PODMEMS system simulated in **Figure 2**.

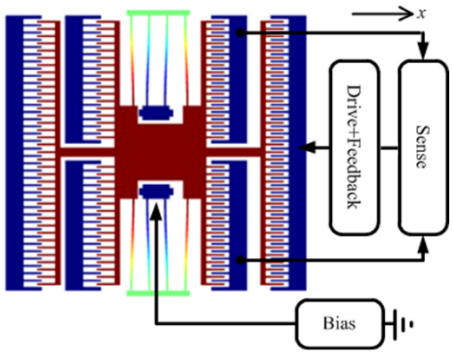

Figure 2: MEMS + performance controller. Symmetric feedback components on the right and left (not shown) sides of the structure operate 180° out of phase for continuous feedback response throughout each cycle. Feedback forces are applied to left and right combs to enhance or oppose displacement, velocity, or acceleration.

The design parameters for the test case shown in **Figure 2** are as follows. Folded flexures have width w = 2μm, thickness h = 20μm, and length L = 294.7μm; two pairs of 100-finger comb drive arrays have finger length L_f = 20μm, finger width w_f = 2μm, and gap g_f = 2μm; Young's modulus E = 160GPa, density ρ = 2300kg/m^3, structure-to-substrate gap $g_{substrate}$ = 2μm, viscosity $\mu = 1.75\times10^{-5}$sPa, and proof mass area $a_m = 1.74\times10^4$ μm^2 (including flexures and combs). This yields a compact mass and stiffness of $M = \rho \times volume = 8\times10^{-10}$ kg, and $K = Ehw^3/4/(L/2)^3 = 2$N/m. The damping at standard atmospheric pressure is $D = \mu a_m / g_{substrate} = 1.55\times10^{-7}$ Ns/m with a quality factor of $Q \approx \omega_0 M/D = 258$. The drive force is $F_{dr} = \left(N\varepsilon h/g_f\right)V_{dr}^2$, where the number of fingers $N = 37$ and the permittivity of the medium is $\varepsilon = 8.854\times10^{-12}$ F/m.

For a driving amplitude of $V_{dr,\max} = 5$V, the linear version of (1), i.e. $\kappa_e = 0$, achieves a displacement amplitude of $x_{\max} = F_{dr}/(\omega_0 D) = 5.28$μm. The nonlinear term in (1) is driven by $F_\kappa = \kappa_e x_\tau^3 = \left(N\varepsilon h/g_f\right)V_\kappa^2$. So the size of the nonlinear coefficient $\kappa_e = V_\kappa^2\, N\varepsilon h/\left(g_f x_{\tau,\max}^3\right)$ is controlled by the feedback voltage V_κ. A family of responses

parameterized by V_κ in **Figure 3**. Spring hardening $\kappa_e > 0$ or softening $\kappa_e < 0$ depends on if the direction of force F_κ is applied in the direction of (or opposite to) displacement $x(t)$.

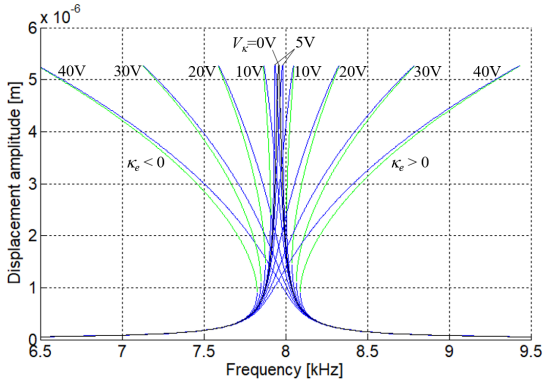

Figure 3: Families of nonlinear responses for a variety of nonlinear stiffness terms, ranging in a variety of feedback voltages V_κ for $\kappa_e = V_\kappa^2 N\varepsilon h / \left(g_f x_{r,\max}^3\right)$. The 5VAC driving voltage of the MEMS results in a displacement amplitude of 5.28μm. The velocity resonance frequency is $f_0 = 7.96$kHz. The blue amplitudes are the stable amplitudes. The green amplitudes are unstable. The vertical pole in the middle is that of the linear version of (1), the traditional response of most MEMS resonators.

3. THERMAL DRIFT

The effect of thermal drift between linear and nonlinear MEMS can differ greatly. We model the effect of changes in temperature on stiffness as the thermal expansion of length, width, and thickness of the flexures as well as the effect of temperature on the Young's modulus (model based on [12]). The double folded-flexure stiffness is

$$K(T) = \frac{E(T)\,h(T)}{4}\left(\frac{w(T)}{\frac{1}{2}L(T)}\right)^3 \tag{2}$$

where

$$L(T) = L_0\left(1+\alpha\,\Delta T\right),$$
$$w(T) = w_0\left(1+\alpha\,\Delta T\right),$$
$$h(T) = h_0\left(1+\alpha\,\Delta T\right), \text{ and}$$
$$E(T) = 145\times10^9\ \exp\left(\frac{2.61\times10^{-3}\,eV}{k_B\,T}\right)\ [\text{Pa}],$$

where the coefficient of thermal expansion of silicon is $\alpha = 2.6\times10^{-6}\ \text{K}^{-1}$, the reference geometry at 300K is L_0, w_0, h_0, electron volts is $eV = 1.6\times10^{-19}\,\text{J}$, and Boltzmann constant is $k_B = 1.38\times10^{-23}\,\text{J/K}$. Ignoring the effect of temperature on the electronics, we plot the frequency response of linear and nonlinear versions of (1) in **Figure 4**, where an increase in temperature of 100K (from 200K to 300K) increases resonance frequency by 91Hz, causing a significant attenuation in amplitude by −84.8% for the linear case and −5.12% for the nonlinear case. Note that the driving frequency of the linear case requires that it matches the mechanical resonance frequency as closely as possible, however; the nonlinear case has an effective wide bandwidth, enabling the driving frequency to be largely detuned by roughly 500Hz.

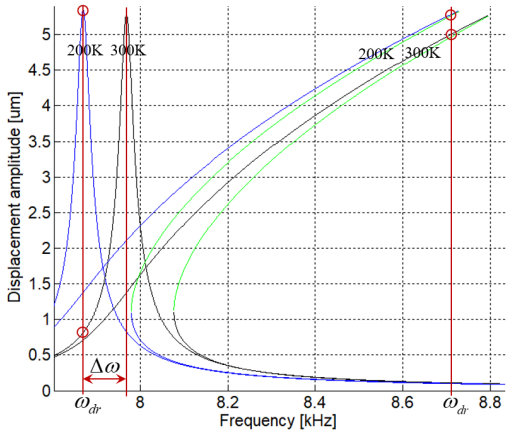

Figure 4: Frequency responses of linear and nonlinear models undergoing thermal drift. Given constant driving frequency of 7.86kHz for the linear case and 8.71kHz for the nonlinear case, a change in temperature of +100K produces a change in amplitude of -84.8% for the linear case and -5.12% for the nonlinear case. The change in amplitude resonance frequency is +91Hz.

4. MISMATCH

The mismatch between the resonance frequencies of two or more resonators (that have originating designs that match) can be due to variations in: fabrication processing, packaging stress, temperatures, damping, etc. The problems of mismatch is quite significant for high-Q resonators due to their narrow bandwidths. This is particularly problematic for vibratory gyros that require the matching of their drive mode (mode-1) with that of their sense mode (mode-2). The better the match between modes 1 and 2, the higher the gyro's signal-to-noise ratio. Mode-2 is driven by mode-1's resonance frequency $\omega_{0,1}$ through the Coriolis force,

$$F_{Coriolis,2} = 2M_2\,\omega_{external}\times\dot{x}_1, \tag{3}$$

where $\dot{x}_1 = \frac{F_{dr,\max,1}}{D_1}\cos\left(\omega_{0,1}\,t\right)$ and $x_1 = \frac{F_{dr,\max,1}}{\omega_{0,1}D_1}\sin\left(\omega_{0,1}\,t\right)$ for the linear case at steady-state.

For instance, let the stiffness of mode-1 be 2% smaller than the stiffness of mode-2 resulting is an 80Hz mismatch. If the system has a high quality-factor Q of 50k (**Figure 1**)

(i.e. D of 8×10^{-10} Ns/m), then operating voltages can be reduced. In this particular case, the driving voltage will be $V_{dr,\max}=1.1\text{V}$ and the nonlinear feedback voltage will be $V_{\kappa}=1\text{V}$. This results in a maximum displacement amplitude of mode-1 of 50.4μm (**Figure 5**), while the maximum amplitude of mode-2 is 7.2nm (**Figure 6**) due to an input earth rate of $\omega_{external}=2\pi/day$. Although the resonance frequencies between the two modes are mismatched, the oscillation frequency of mode-1 can be detuned to precisely match the resonant frequency of mode-2.

A system-level block diagram of the PODMEMS system is shown in **Figure 7**. The BJT cubic nonlinearity block is tuned as $i_{out}=\left(i_1/i_2^3\right)i_{in}^3$, where i_{in} is proportional to the displacement of the proof mass.

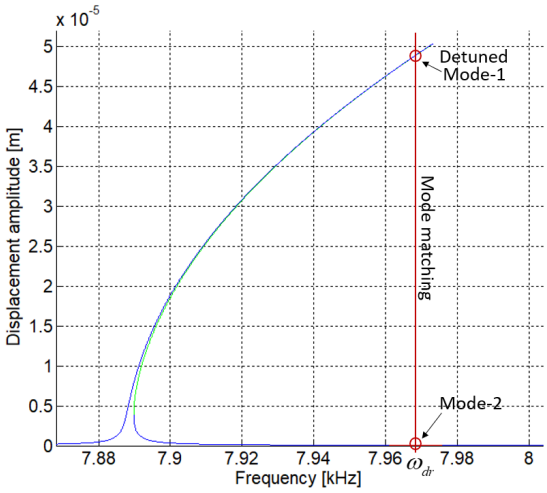

Figure 5: Frequency responses for mismatched mode-1 (drive mode) and mode-2 (sense mode) of a vibratory gyro model. Due to the bent pole of mode-1, its driving frequency can be detuned to precisely match the resonance frequency of mode-2. The response of mode-2 is shown magnified in Figure 6.

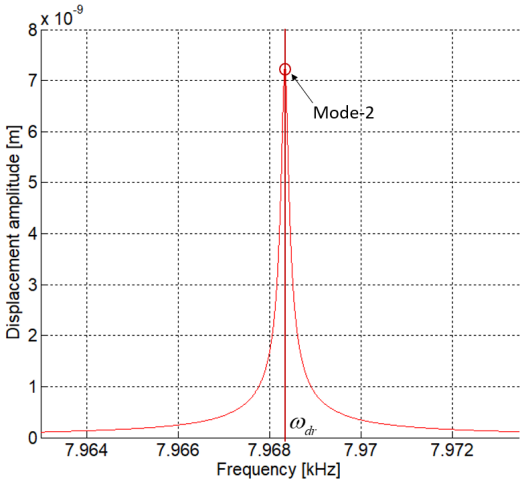

Figure 6: Frequency response of mode-2 (magnified Figure 5).

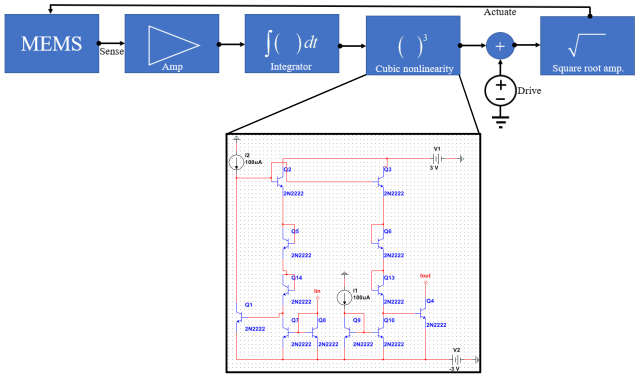

Figure 7: Block diagram for nonlinear stiffness control.

5. Conclusion

In this paper we explored how performance control feedback can be used to produce Duffing-like behavior for small deflection amplitudes that are traditionally linear. We developed a method for controlling the amount of nonlinearity in stiffness. Our modeling results suggest that such nonlinear behavior might be a useful option to consider when addressing the problems of drift or mismatch.

References

[1] I. P. Prikhodko, B. R. Simon, G. Sharma, S. A. Zotov, A. A. Trusov, A. M. Shkel, "High and moderate-level vacuum packaging of vibratory MEMS", *International Symposium on Microelectronics*, Sept. 30, 2013, pp.705-710.

[2] R. M'Closkey, A. Vakakis, "Analysis of a microsensor automatic gain control loop", *In Proceedings of the American Control Conference*, San Diego, CA, USA, June 2-4, 1999, pp. 3307-3311.

[3] X. Sun, R. Horowitz, K. Komvopoulos, "Stability and resolution analysis of a phase-locked loop natural frequency tracking system for MEMS fatigue testing", *J. Dyn. Syst. Meas. Control*, 2002, Vol. 124, pp. 599-605.

[4] S. Park, R. Horowitz, "New adaptive mode of operation for MEMS gyroscopes", *J. Dyn. Syst. Meas. Control* 2004, Vol. 126, pp. 800-810.

[5] P. Sungsu, C.-W. Tan, H. Kim, and S. K. Hong, "Oscillation Control Algorithms for Resonant Sensors with Applications to Vibratory Gyroscopes", *Sensors* 2009, Vol. 9, 5952-5967.

[6] F. Yesil, S. E. Alper, and T. Akin, "An Automatic Mode Matching System for a High *Q*-Factor MEMS Gyroscope Using A Decoupled Perturbation Signal", *Transducers*, June 2015, pp.1148-1151.

[7] D. Kim and R. M'Closkey, "A MEM vibratory gyro with mode-matching achieved by resonator mass loading," *2014 IEEE/ION Position, Location and Navigation Symposium - PLANS*, Monterey, CA, May 2014, pp. 499-503.

[8] F. Bu, D. Xu, H. Zhao, B. Fan, M. Cheng, "MEMS Gyroscope Automatic Real-Time Mode-Matching Method Based on Phase-Shifted 45° Additional Force Demodulation", *Sensors*, 2018; Vol. 18 No. 9, pp. 1-6.

[9] A. H. Nayfeh, B. Balachandran, *Applied Nonlinear Dynamics: Analytical, Computational, and Experimental Methods*, Wiley-VCH, 2004.

[10] B. Balachandran, T. Kalmár-Nagy, D. E. Gilsinn, *Delay Differential Equations: Recent Advances and New Directions*, Springer, 2009.

[11] J. V. Clark, O. Misiats, S. Sayed, "Electrical control of effective mass, damping, and stiffness of MEMS devices", *IEEE Sensors Journal*, 2017, Vol. 17, No. 5, pp. 1363-1372.

[12] K. Shirai, "Temperature Dependence of Young's Modulus of Silicon", *Japanese Journal of Applied Physics*, Aug. 2013, Vol. 52.